Range Ambiguity Resolution and DoA Estimation Enhancement in MIMO SC-FDMA Systems

Chanul Park, Seonmin Cho, and Seongwook Lee Department of Electrical and Electronics Engineering College of ICT Engineering, Chung-Ang University Seoul, Republic of Korea {qkrcksdnf97, tjsals4514, seongwooklee}@cau.ac.kr

Abstract—This paper proposes a method to enhance direction of arrival (DoA) estimation accuracy and resolve range ambiguity in interleaved subcarrier-based multiple-input multiple-output (MIMO) single carrier-frequency division multiple access (SC-FDMA) systems for radar applications. Using the virtual array in the MIMO configuration, a large effective aperture can be synthesized using a relatively small number of transmitting and receiving antenna elements, enabling high angular resolution. To realize this virtual array, orthogonality among multiple transmitters must be ensured. For instance, the interleaved subcarrier allocation scheme enables signals from multiple transmitting antenna elements to be orthogonal. However, this allocation introduces range-dependent phase shifts between transmitting antenna elements, which degrade DoA estimation accuracy, and reduces the maximum unambiguous detection range. To mitigate these problems, we propose a method to compensate for the phase shift in each virtual array, along with a range ambiguity resolution method based on phase linearity analysis. The proposed methods are validated through simulations. With the proposed method, the average DoA estimation error is reduced from 5.63° to 0.2°. Furthermore, the proposed method successfully resolves range ambiguity, reducing the estimation error to 0 m for a target at 1500 m, which lies beyond the system's maximum unambiguous range of 384 m. The results confirm that the proposed approach improves DoA estimation accuracy and resolves range ambiguity in interleaved MIMO SC-FDMA systems.

Index Terms—integrated sensing and communications (ISAC), multiple-input multiple-output (MIMO), single carrier-frequency division multiple access (SC-FDMA).

I. INTRODUCTION

The growing demand for spectrum-efficient wireless systems has sparked significant interest in integrated sensing and communications (ISAC) systems, which enable simultaneous radar sensing and wireless communications within a single platform [1], [2]. Among various waveform candidates for ISAC systems, the orthogonal frequency division multiplexing (OFDM)-based system has gained considerable attention due to its inherent compatibility with modern communication standards and its ability to perform radar sensing operations [3], [4]. However, despite these benefits, OFDM-based ISAC system suffers from a high peak-to-average power ratio (PAPR) [5]. The high PAPR characteristic of OFDM signals poses significant challenges in practical implementations, particularly for uplink communications and mobile device applications. High PAPR requires linear power amplifiers with large backoff margins to avoid signal distortion, leading to reduced

power efficiency and increased hardware complexity. This limitation becomes especially problematic in battery-powered devices and cost-sensitive ISAC applications, where power consumption and hardware costs are critical design constraints. To address these challenges, single carrier-frequency division multiple access (SC-FDMA) has emerged as an attractive alternative. SC-FDMA maintains the fundamental advantages of OFDM while significantly reducing PAPR by employing a precoding operation that transforms the multicarrier signal into a single carrier-like waveform [6], [7]. This approach enables the use of more efficient, less expensive power amplifiers without sacrificing spectral efficiency or system performance. The reduced PAPR characteristics of SC-FDMA translate directly into practical benefits for radar application. Lower PAPR requirements allow for the use of non-linear power amplifiers with smaller back-off margins, resulting in improved power efficiency and reduced hardware costs [8]. This enables the design of more efficient hardware architectures. Consequently, SC-FDMA is well-suited for applications where power consumption and cost-effectiveness are critical, such as mobile ISAC, automotive sensing, and distributed ISAC networks.

Building upon these motivations, this paper investigates multiple-input multiple-output (MIMO) SC-FDMA systems for radar sensing. MIMO array configurations are essential for high-resolution direction of arrival (DoA) estimation through the formation of virtual arrays, which significantly expand the effective aperture size beyond the physical antenna constraints and enable superior spatial resolution capabilities. To ensure orthogonality among multiple transmitting antenna elements, interleaved subcarriers are allocated to each transmit antenna element. However, the interleaved subcarrier allocation scheme introduces specific challenges that must be addressed. One significant issue is the degradation of DoA estimation accuracy caused by frequency offsets between different transmitting antenna elements. In addition, the use of interleaved subcarriers results in a reduction in the maximum unambiguous range. This range limitation increases the likelihood of phase wrapping effects, where targets beyond the unambiguous range appear as ghost targets at incorrect range positions. Such range ambiguity issues can severely compromise the reliability of target detection and tracking in practical scenarios. To address these challenges, this paper proposes comprehensive solutions that simultaneously tackle both DoA estimation

accuracy degradation and range ambiguity problems in interleaved MIMO SC-FDMA systems. The proposed techniques aim to compensate for frequency offset-induced phase errors while providing effective range ambiguity resolution methods, thereby enabling robust and accurate target detection across extended operating ranges.

II. SIGNAL MODEL OF SC-FDMA SYSTEMS

A. Range and Velocity Estimation

To simplify the notation, we consider a single-input single-output (SISO) SC-FDMA system. A single transmit antenna element transmits modulated symbols that have been processed with discrete Fourier transform (DFT) spreading. Let N_c be the total number of subcarriers and N_s be the number of SC-FDMA symbols in a single frame. For each time index $n \in \{0,1,\ldots,N_c-1\}$ and symbol index $s \in \{0,1,\ldots,N_s-1\}$, let X[n,s] be the data symbol drawn from an M-ary quadrature amplitude modulation (QAM) (or an equivalent modulation scheme) that is fed into the DFT precoder. The modulated symbol sequence is first transformed using the N_c -point DFT. The DFT output $\tilde{X}[k,s]$ is given by

$$\tilde{X}[k, s] = \sum_{n=0}^{N_c - 1} X[n, s] \exp\left(-j\frac{2\pi}{N_c}kn\right). \tag{1}$$

Next, an inverse DFT transforms the frequency-domain signal into the time-domain baseband signal, which can be expressed as

$$x[n, s] = \frac{1}{N_c} \sum_{k=0}^{N_c - 1} \tilde{X}[k, s] \exp\left(j\frac{2\pi}{N_c} kn\right).$$
 (2)

The signal is then up-converted to a radio frequency (RF) carrier at frequency f_c . This results in a passband transmit signal $x_{\rm RF}(t)$, which can be expressed as

$$x_{\rm RF}(t) = x[n, s] \exp(j2\pi f_c t), \tag{3}$$

where $t=nT_c+sT_s$, and T_c and T_s denote sampling period and symbol duration, resepectively. The transmitted signal propagates toward a single point target and is reflected back to the receiver. This two-way path induces a round-trip delay of $\tau=2R/c$ and a Doppler frequency $f_D=2vf_c/c$, where $R,\,V$, and c denote the target range, velocity, and the speed of light, respectively. The received RF signal after reflection from the target is modeled as

$$y_{\rm RF}(t) = \sigma x_{\rm RF}(t-\tau) \exp\left(j2\pi f_D(t-\tau)\right),\tag{4}$$

where σ is the complex amplitude proportional to the target radar cross section (RCS). The received signal is then down-converted to baseband and sampled at $t = nT_c + sT_s$. The resulting baseband signal can be expressed as

$$y[n, s] = \sigma x[n - n_{\tau}, s] \exp(j2\pi f_D(nT_c + sT_s)),$$
 (5)

where $n_{\tau}=\tau/T_c$ represents the discrete sample delay corresponding to the round-trip propagation delay 2R/c.

Finally, the receiver applies an N_c -point DFT to y[n, s] to recover the frequency-domain received signal. The output at subcarrier k is given by

$$Y[k, s] = \sum_{n=0}^{N_c - 1} y[n, s] \exp\left(-j\frac{2\pi}{N_c}kn\right).$$
 (6)

To suppress the effect of the transmitted waveform and perform matched filtering, spectral equalization is applied by

$$\tilde{Y}[k, s] = Y[k, s]\tilde{X}^*[k, s]. \tag{7}$$

Next, we perform an inverse DFT across the subcarrier dimension to obtain the range profile, which can be expressed

$$\tilde{Y}_{\text{range}}[r, s] = \frac{1}{\sqrt{N_c}} \sum_{k=0}^{N_c - 1} \tilde{Y}[k, s] \exp\left(j\frac{2\pi}{N_c}kr\right),$$
 (8)

where $r \in \{0, ..., N_c - 1\}$ is the range bin index. Then, a DFT is performed along the SC-FDMA symbol dimension to estimate the Doppler shift, which can be expressed as

$$\tilde{Y}_{\text{range-Doppler}}[r, v] = \frac{1}{\sqrt{N_s}} \sum_{s=0}^{N_s - 1} \tilde{Y}_{\text{range}}[r, s] \exp\left(-j\frac{2\pi}{N_s}sv\right),$$
(9)

where $v \in \{0, \ldots, N_s - 1\}$ is the Doppler (i.e., velocity) bin index. The final two-dimensional output $\tilde{Y}_{\text{range-Doppler}}$ contains the joint range and velocity information of the target.

B. DoA Estimation in MIMO Arrays

Under far-field assumption, the incoming wavefront can be approximated as a plane wave, such that all antenna elements experience the same DoA. Fig. 1 illustrates this concept, where the signals received at adjacent receiving antenna elements have an additional path difference of $d_{\rm ant} \sin \theta$, resulting in a phase difference of $\frac{2\pi}{\lambda} d_{\rm ant} \sin \theta$ [9]. Consequently, the DoA can be estimated from the phase differences between the signals received at each antenna element. In this context, the angular resolution of the MIMO system is proportional to the number of receiving antenna elements. However, increasing the number of physical antenna elements significantly raises system cost and complexity. To address this, a MIMO configuration can be employed to form a virtual array, enabling the system to achieve the effect of having a large number of receiving elements while physically using fewer antennas.

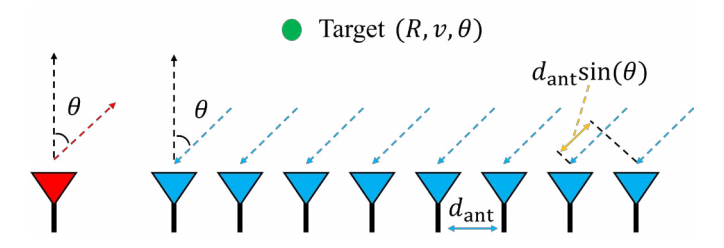


Fig. 1. Illustration of path difference between adjacent elements in a linear antenna array.

Fig. 2 illustrates examples of MIMO and single-input multiple-output (SIMO) arrays. A system with 2 transmitting and 4 receiving antenna elements can form a virtual uniform linear array (ULA) equivalent to an 8-element receive array. This is achieved by setting the transmit antenna spacing to be four times the receive antenna spacing. This enables the system to achieve the same DoA resolution as a 1×8 array antenna system while using only 6 antenna elements. The DoA estimation procedure in the MIMO system is as follows. First, the target's range and velocity are detected in the twodimensional range-Doppler domain. This is accomplished using a peak detection technique, such as the constant false alarm rate method [10]. For each detected peak, the corresponding complex values from all elements of the virtual array are collected and form a signal vector [11], as shown in Fig. 3. Subsequently, a covariance matrix is constructed from the extracted signal vector, and DoA estimation is performed using algorithms such as the conventional beamformer [12], minimum variance distortionless response [13], or multiple signal classification (MUSIC) [14].

III. PROPOSED METHOD FOR RANGE AMBIGUITY RESOLUTION AND DOA ESTIMATION ENHANCEMENT

In the proposed MIMO SC-FDMA system, orthogonality between transmitting antenna elements is ensured by allocating distinct sets of subcarriers to each transmitting antenna element. This approach enables simultaneous transmission

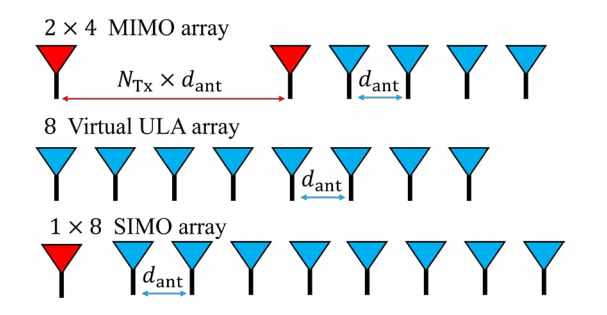


Fig. 2. Illustration of a MIMO antenna configuration, the corresponding virtual array, and the equivalent SIMO array.

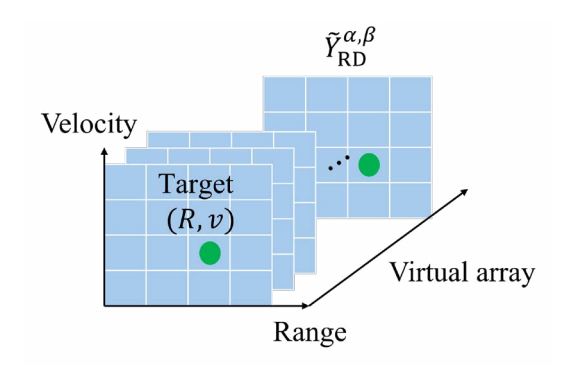


Fig. 3. Extraction of signal vector along the virtual array axis of the range-Doppler map for DoA estimation.

from multiple antenna elements without mutual interference. Hence, a virtual array can be synthesized at the receiving end. Two representative subcarrier allocation schemes are commonly considered in MIMO SC-FDMA systems: interleaved and localized allocation, as shown in Fig. 4 [8]. In the interleaved scheme, each transmitting antenna element uses every $N_{\rm TX}$ -th subcarrier in a round-robin manner across the entire bandwidth. Alternatively, the localized scheme uses a contiguous block of subcarriers for each transmitting antenna element. Although both schemes offer transmit orthogonality, the interleaved structure preserves the full range resolution due to its wide frequency span, making it more suitable for high-resolution radar sensing. Therefore, we adopt the interleaved subcarrier allocation in our system design.

When distinct subcarriers are assigned to each transmitting antenna elements in the interleaved MIMO SC-FDMA scheme, the received signal corresponding to each transmitting-receiving pair experiences a subcarrier-dependent phase shift. This shift is caused by two factors: the spatial position of the virtual antenna and the time delay from the target reflection. Specifically, the received signal includes a multiplicative phase term given by

$$H_{\alpha,\beta}[k] = \sigma \exp\left(-j\frac{2\pi}{\lambda}d_{\text{ant}}u_{\alpha,\beta}\sin\theta\right) \times \exp\left(-j2\pi\tau f_s\alpha\right), \tag{10}$$

where σ_p is the RCS of the target and $u_{\alpha,\beta} = \alpha N_{\rm RX} + \beta$ represents the virtual antenna index corresponding to transmitting antenna elements α ($\alpha = 0, 1, \dots, N_{TX}$) and receiving antenna elements $\beta\,(\beta\,=\,0,\,1,\,\cdots,\,N_{\rm RX}).$ In (10), the first exponential term accounts for the DoA-dependent phase difference caused by the spatial separation between receiving antenna elements. The second exponential term represents the frequency-dependent phase shift induced by the time delay. This frequency dependence arises because the interleaved subcarrier allocation causes the effective center frequency to vary for each transmitting antenna. This causes a phase shift across the virtual array, which can distort accurate DoA estimation without proper compensation [15]. To mitigate this distortion, we apply a phase compensation method before DoA estimation. Let (r_p, v_p) denote the range and Doppler bin indices corresponding to the p-th detected target in the

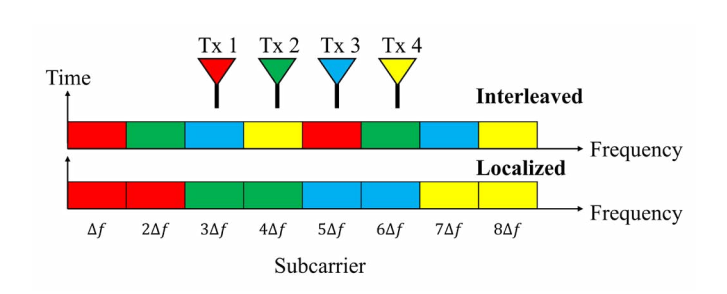


Fig. 4. Illustration of interleaving and localized subcarrier allocation schemes for MIMO SC-FDMA system.

range-Doppler map. The value $r_p \in \{0, 1, \ldots, N_{\rm c} - 1\}$ indicates the range bin where the target is located and while $v_p \in \{0, 1, \ldots, N_{\rm s} - 1\}$ denotes the associated Doppler bin index.

To compensate for this phase shift across transmitting antenna elements at the detected range bin r_p , we apply the following phase compensation factor to each transmitting antenna element, which can be expressed as

$$\phi_{\alpha}[r_p] = \exp\left(j2\pi \frac{N_{\rm TX} - \alpha - 1}{N_{\rm TX}} \frac{2f_s r_p \Delta R}{c}\right), \qquad (11)$$

where $r_p\Delta R$ is an estimated discrete range associated with the detected range bin and $\Delta R=c/2B$ is range resolution. The compensation vector $\boldsymbol{\phi}[r_p]$ is applied through elementwise multiplication to the signal vector. The phase-corrected signal vector is expressed as

$$\tilde{\mathbf{y}}_{\text{virtual}}[r_p, q_p] = \mathbf{y}_{\text{virtual}}[r_p, q_p] \odot \boldsymbol{\phi}[r_p],$$
 (12)

where \odot denotes the element-wise product and $\phi[r_p]$ is the vector of compensation factors applied to each virtual antenna element. In addition, $\mathbf{y}_{\text{virtual}}[r_p,q_p]$ is the signal vector extracted from $\tilde{Y}_{\text{range-Doppler}}$ along the virtual array axis. After this compensation, subspace-based DoA estimation algorithms such as MUSIC can be applied. However, when a target lies beyond the maximum unambiguous range, phase wrapping results in an estimated range that differs from the true range to the target. In such cases, applying the phase compensation factor based on r_p does not result in a linear phase progression across the virtual array, leading to inaccurate DoA estimation. For interleaved MIMO systems, this problem becomes acute because the maximum unambiguous range $R_{\max} = \frac{c}{2f_s N_{\mathrm{TX}}}$ decreases in proportion to the number of transmit antenna elements

To address this, we evaluate the phase alignment after each phase compensation. If the compensated virtual array still exhibits non-linear phase, we hypothesize that the true range is located in the next unambiguous interval, i.e., $r_p\Delta R + R_{\rm max}.$ The phase compensation is then recalculated using this extended range. This process is repeated with the successive additions of $R_{\rm max}$ until a linear phase progression is achieved. Once a consistent linear phase is obtained across the virtual array, the target range is estimated as $R_p = r_p\Delta R + R_{\rm max}.$ Consequently, the range ambiguity is resolved.

IV. PERFORMANCE EVALUATION

A. Parameters of SC-FDMA System Used in Simulation

To verify the effectiveness of the proposed method, simulations were conducted. The specifications of the SC-FDMA radar employed in the simulation are as follows. The carrier frequency is set to 28 GHz, and the total system bandwidth is 400 MHz. This bandwidth is partitioned into 4096 subcarriers, resulting in a subcarrier spacing of 97.65 kHz. The number of SC-FDMA symbols per frame is set to 1024. We configured the MIMO system with 8 receiving antenna elements and 4 transmitting antenna elements. The spacing between the receiving antenna elements is configured as half the wavelength.

For the 28 GHz carrier frequency, this corresponds to 5 mm. The transmitting antenna elements are then spaced 4 times the spacing between receiving antenna elements, resulting in a 2 cm seperation. The range resolution is given by $\Delta R = \frac{c}{2B} = 0.375$ m, and the unambiguous maximum range is 384 m. The simulation parameters used for the MIMO SC-FDMA system are summarized in Table I.

B. Qualitative Evaluation

The simulation scenario considered two point targets. The first target is located at a range of 200 m and an azimuth angle of 10.3°, with a radial velocity of -50 m/s. The second target is located at a range of 665 m an azimuth angle of 30°, with a radial velocity of 30 m/s. Fig. 5 shows the RV map, where the two targets are indicated by red circles. The first target is detected at its designated position, whereas the second target, located at 665 m, exceeds the maximum unambiguous detection range of 384 m and thus appears at an aliased position corresponding to 280.87 m in the range-Doppler map. Fig. 6 presents the results of phase analysis obtained from the signal vector of the first target along the virtual array axis. The phases are ordered according to the virtual array element index and subsequently unwrapped. Before phase compensation, the signal received from the same transmit antenna element

TABLE I
SIMULATION PARAMETERS FOR MIMO SC-FDMA SYSTEM

Parameter	Value
Carrier frequency, f_c	28 GHz
Bandwidth, B	400 MHz
The total number of subcarriers, N_c	4096
Subcarrier spacing, f_s	97.65 kHz
SC-FDMA symbols per frame, N_s	1024
Symbol duration, T_s	10.24 μ s
Modulation scheme	16-QAM
The number of transmit antenna elements, $N_{\rm TX}$	4
The number of receive antenna elements, $N_{\rm RX}$	8
Transmitting antenna element spacing	2 cm
Receiving antenna element spacing, d_{ant}	5 mm
The number of virtual antennas, N_{virtual}	32

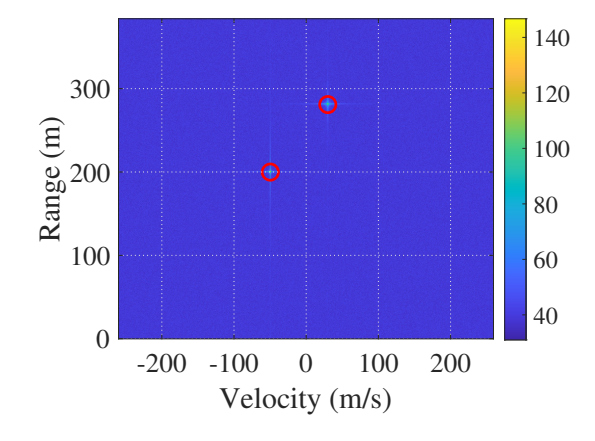


Fig. 5. Range-Doppler map with two peaks at (199.87 m, -50 m/s) and (280.87 m, 30 m/s).

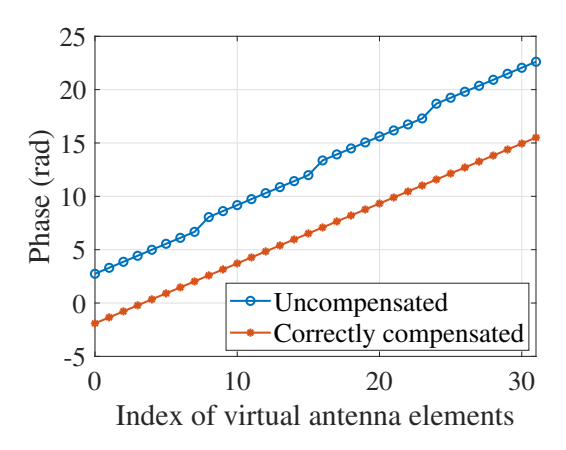


Fig. 6. Unwrapped phase of the virtual array signal vector before and after phase compensation for the target located at (199.87 m, -50 m/s).

exhibited a linear phase trend along the virtual array axis, whereas a phase discontinuity occurs whenever the transmit antenna changes. After the phase compensation is applied, the phases exhibit a linear trend across all elements of the virtual array. Subsequently, the DoA is estimated using the MUSIC algorithm. The results are shown in Fig. 7. As shown in the figure, before applying phase compensation, the estimated DoA is 12.1°. After applying the compensation based on the target range and transmit antenna element index, the estimated DoA changed to the actual truth value of 10.3°.

Fig. 8 shows the target phase estimated at 280.87 m. As shown in the figure, the uncompensated phase contains discontinuities. After applying compensation based on the estimated range of 280.87 m, the phase still exhibits discontinuities. This indicates that range ambiguity has occurred and that the applied phase compensation is incorrect. To resolve this ambiguity, we added the maximum unambiguous range to the initial estimate, obtaining 664.5 m. By applying the phase compensation term configured with this ambiguity-aware range,

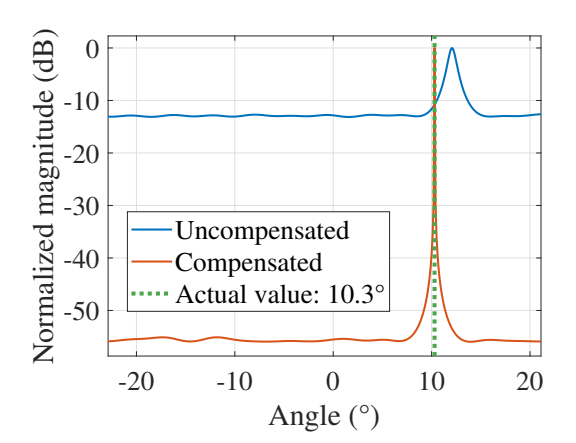


Fig. 7. MUSIC-based DoA estimation results before and after phase compensation for target at (199.87 m, -50 m/s).

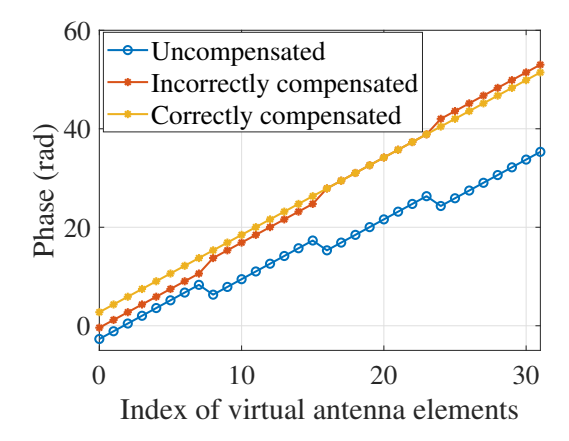


Fig. 8. Unwrapped phase, before and after phase compensation, obtained by collecting the signals at (280.87 m, 30 m/s) from all receiving antennas and arranging them along the virtual array axis.

the phase becomes linear. This shows that range ambiguity can be resolved by checking whether phase discontinuities between virtual array elements disappear after compensation. As illustrated in Fig. 9, the MUSIC-based DoA estimation was evaluated for three scenarios: uncompensated, compensated by 280.87 m, and compensated by 664.5 m. In the absence of compensation, the estimated DoA is 32.9°. Applying a 280.87 m compensation yields 33.9°, which still deviates from the actual truth. Applying the 280.87 m compensation produces an incorrect estimate of 33.9°. In contrast, the 664.5 m compensation results in 30°, which matches the actual truth.

C. Quantitative Evaluation

To evaluate the proposed method's performance in DoA estimation and range ambiguity resolution with respect to target distance, we performed simulations at 37.5 m intervals for distances ranging from 0 to 1500 m. The results are shown in Fig. 10. Before applying the phase error compensation,

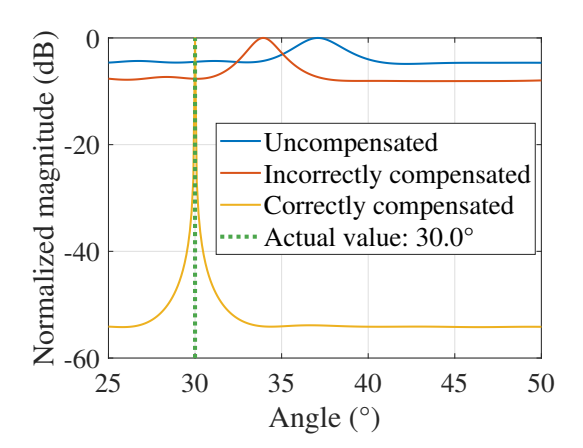


Fig. 9. MUSIC-based DoA estimation results before and after phase compensation for target at ($280.87\ m,\ 30\ m/s$).

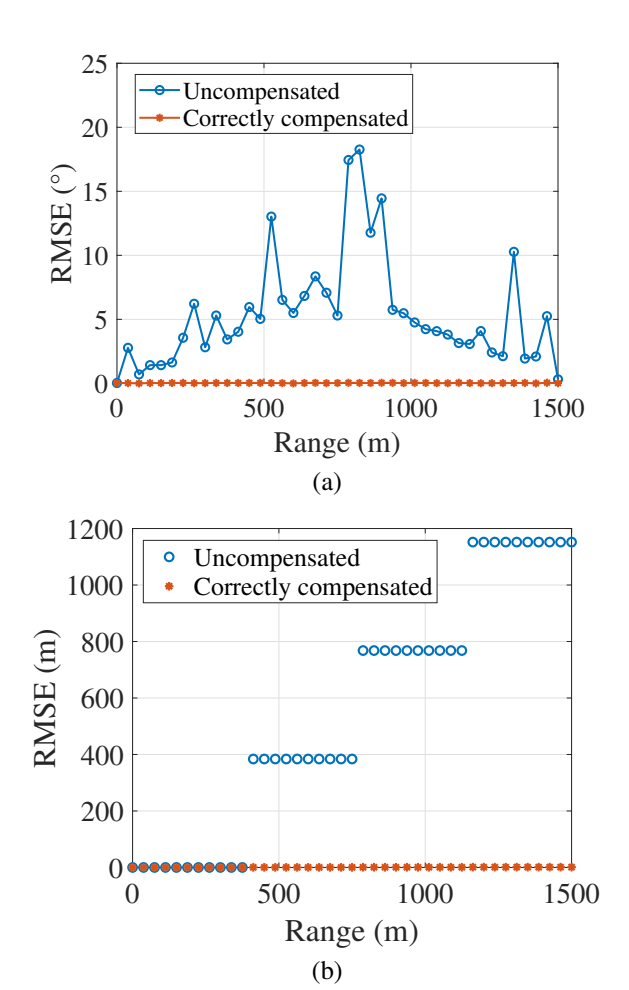


Fig. 10. RMSE with and without using the proposed method: (a) DoA estimation and (b) range estimation.

the average RMSE of DoA estimation was 5.63°, whereas it was reduced to 0.2° after applying the proposed method, as shown in Fig. 10 (a). The conventional SC-FDMA system suffered from range ambiguity errors, with a maximum RMSE of 1152 m. In contrast, the proposed method eliminated these errors, reducing the average range estimation RMSE to 0 m. This result is shown in Fig. 10 (b). These results demonstrate that the proposed method effectively addresses the two major drawbacks of subcarrier-interleaving-based MIMO SC-FDMA systems, namely the increased DoA estimation error and the reduced maximum unambiguous range.

V. CONCLUSION

This paper presented a method to enhance DoA estimation accuracy and resolve range ambiguity in interleaved subcarrier-based MIMO SC-FDMA systems for radar applications. The interleaved allocation scheme can provide orthogonality among multiple transmitting antenna elements. However, the resulting frequency offsets dependent on the transmitting antenna element introduced range-dependent phase shifts, affecting the accuracy of the DoA estimation. To address this,

a phase compensation method is proposed. In addition, a range ambiguity resolution strategy was proposed by evaluating the linearity of the compensated phase profile. Simulation results demonstrated that the proposed methods effectively allows accurate DoA estimation can resolve range ambiguity.

ACKNOWLEDGMENT

This work was supported by Institute of Information and Communications Technology Planning and Evaluation (IITP) Grant funded by the Korea government (MSIT) (No. RS-2024-00347032, Development of PMCW-based MIMO Digital Radar SoC for Next-Generation Autonomous Driving).

REFERENCES

- [1] F. Liu, C. Masouros, A. P. Petropulu, H. Griffiths, and L. Hanzo, "Joint radar and communication design: applications, state-of-the-art, and the road ahead," *IEEE Transactions on Communications*, vol. 68, no. 6, pp. 3834–3862, June 2020.
- [2] F. Liu, Y. Cui, C. Masouros, J. Xu, T. X. Han, Y. C. Eldar, and S. Buzzi, "Integrated sensing and communications: toward dual-functional wireless networks for 6G and beyond," *IEEE Journal on Selected Areas in Communications*, vol. 40, no. 6, pp. 1728–1767, June 2022.
- [3] C. Sturm, T. Zwick, and W. Wiesbeck, "An OFDM system concept for joint radar and communications operations," VTC Spring 2009 - IEEE 69th Vehicular Technology Conference, Barcelona, Spain, April 2009, pp. 1-5
- [4] T. Jeong, C. Park, and S. Lee, "Geometric-sequence-decomposition-based joint range and velocity estimation in OFDM radar system for UAM applications", *IEEE Internet of Things Journal*, vol. 11, no. 9, May 2024.
- [5] S. H. Dokhanchi, B. S. Mysore, K. V. Mishra, and B. Ottersten, "A mmWave automotivejoint radar-communications system," *IEEE Transactions on Aerospace and Electronic Systems*, vol. 55, no. 3, pp. 1241-1260, June 2019.
- [6] A. Hajisami, J. Lansford, A. Dingankar, and J. Misener, "A tutorial on the LTE-V2X directcommunication," *IEEE Open Journal of Vehicular Technology*, vol. 3, pp. 388–398, August 2022.
- [7] V. Jungnickel, T. Hindelang, T. Haustein, and W. Zirwas, "SC-FDMA waveform design, performance, power dynamics and evolution to MIMO," 2007 IEEE International Conference on Portable Information Devices, Orlando, FL, USA, May 2007, pp. 1–6.
- [8] R. Saadia and N. M. Khan, "Single carrier-frequency division multiple access radar: waveformdesign and analysis," *IEEE Access*, vol. 8, pp. 35742–35751, February 2020.
- [9] H. Park, C. Park, S. Kwak, and S. Lee, "MIMO FMCW radar-based indoor mapping through exploiting multipath signals", *IEEE Internet of Things Journal*, vol. 11, no. 19, pp. 31479–31491, October 2024.
- [10] C. Park, S. Kwak, H. Lee, and S. Lee, "Bidirectional LSTM-based overhead target classification for automotive radar systems", *IEEE Transac*tions on Instrumentation and Measurement, vol. 73, pp. 1–11, December 2023
- [11] H. Lee, S. Kwak, and S. Lee, "Multiple-output network for simultaneous target classification and moving direction estimation in automotive radar systems," *Expert Systems with Applications*, vol. 259, no. 125280, pp. 1–14, January 2025.
- [12] C. Park, H.-I. Baek, Y. Chae, H.-S. Lim, J.-E. Lee, and S. Lee, "Deep-learning-based kick motion recognition in millimeter waveband radar system," *IEEE Sensors Journal*, vol. 24, no. 19, pp. 31395–31407, October 2024.
- [13] J. Capon, "High-resolution frequency-wavenumber spectrum analysis," Proceedings of the IEEE, vol. 57, no. 8, pp. 1408–1418, August 1969.
- [14] R. O. Schmidt, "Multilinear array manifold interpolation," *IEEE Transactions on Signal Processing*, vol. 40, no. 4, pp. 857–866, April 1992.
- [15] T. Multerer, U. Prechtel, M. Vossiek, and V. Ziegler, "Systematic phase correction for direction-of-arrival estimation in spectrally interleaved OFDM MIMO radar," *IEEE Transactions on Microwave Theory and Techniques*, vol. 67, no. 11, pp. 4570–4577, November 2019.